Critical phenomena in gravitational collapse with two competing massless matter fields

Carsten Gundlach
Mathematical Sciences, University of Southampton, Southampton SO17 1BJ, United Kingdom

Thomas W. Baumgarte
Department of Physics and Astronomy, Bowdoin College, Brunswick, Maine 04011, USA

David Hilditch
CENTRA, Departamento de Física, Instituto Superior Técnico IST, Universidade de Lisboa UL, Avenida Rovisco Pais 1, 1049 Lisboa, Portugal

(Received 16 August 2019; published 7 November 2019)

In the gravitational collapse of matter beyond spherical symmetry, gravitational waves are necessarily present. On the other hand, gravitational waves can collapse to a black hole even without matter. One might therefore wonder whether the interaction and competition between the matter fields and gravitational waves affect critical phenomena at the threshold of black hole formation. For a toy model for this, we study type II critical collapse with two matter fields in spherical symmetry, namely a scalar field and a Yang-Mills field. On their own, both display discrete self-similarity in type II critical collapse, and we can take either one of them as a toy model for gravitational waves. To our surprise, in numerical time evolutions, we find that, for sufficiently good fine-tuning, the scalar field always dominates on sufficiently small scales. We explain our results by the conjectured existence of a "quasidiscretely self-similar" (QSS) solution shared by the two fields, equal to the known Yang-Mills critical solution at infinitely large scales and the known scalar field critical solution (the Choptuik solution) at infinitely small scales, with a gradual transition from one field to the other. This QSS solution itself has only one unstable mode and so acts as the critical solution for any mixture of scalar field and Yang-Mills initial data.

DOI: 10.1103/PhysRevD.100.104010

I. INTRODUCTION

In simple self-gravitating systems in spherical symmetry, such as a scalar field [1] or ultrarelativistic perfect fluid [2], the time evolution of initial data which are close to the threshold of black hole formation, but otherwise generic, displays certain universal features which are called (type II) critical phenomena in gravitational collapse. In particular, on the supercritical (black hole–forming) side of the threshold, the black hole mass becomes arbitrarily small as the threshold is approached, while on the subcritical (dispersing) side of the threshold, the maximal curvature that occurs during the evolution becomes arbitrarily large. Let p be any smooth parameter of the initial data such that, for all other parameters held fixed, a black hole is formed precisely for $p > p_*$. Then, the black hole mass scales as $(p - p_*)^\gamma$, and the maximum curvature scales as $(p_* - p)^{-2\gamma}$, for some universal critical exponent $\gamma > 0$.

Critical phenomena in gravitational collapse in such simple systems are explained by the existence of a critical solution, which has the key properties that it is regular and self-similar and has precisely one unstable perturbation mode. This solution appears as an intermediate attractor in the time evolution of near-critical initial data. The effect of fine tuning p to its critical value p_* in any one-parameter family is to tune the amplitude of the one unstable mode to zero. In the limit of perfect fine-tuning, the critical solution persists to arbitrarily small scales and correspondingly large curvature, and a naked singularity is formed. Hence, type II critical collapse, at least in the known examples in spherical symmetry, indicates strongly that cosmic censorship holds only for generic initial data but is violated by a set of initial data that in some sense has codimension 1 (see, e.g., Ref. [3] for a review).

It is of great interest to explore whether the critical collapse scenario continues to hold beyond spherical symmetry and, in particular, in the presence of angular momentum or in the collapse of gravitational waves in vacuum.

Going beyond spherical symmetry, we have investigated critical phenomena in gravitational collapse for rotating [4] and nonrotating [5] perfect fluids in axisymmetry. The critical collapse of an axisymmetric scalar field has been investigated in Refs. [6] and [7]; see also Refs. [8–10]. Critical phenomena in axisymmetric vacuum collapse were

 © 2019 American Physical Society

reported in Ref. [11] and partly confirmed much more recently in Ref. [12]; see also Refs. [13–17] for other attempts in the interval between these two papers.

The vacuum case is the most interesting, since it mostly cleanly displays the matter-independent properties of general relativity—but it also appears to be the most difficult numerically. This brings us back to axisymmetric matter models. In these, however, gravitational waves are always also necessarily present. Therefore, critical collapse cannot be moderated by a single critical solution. The obvious conservative scenario has two separate critical solutions dominated by the matter content and by gravitational waves, respectively. But more exotic scenarios are possible, and one of these will be illustrated in this paper.

For a toy model for *axisymmetric* systems with two wavelike degrees of freedom (matter and gravitational waves), we investigate here a system with two wavelike matter degrees of freedom in *spherical* symmetry, namely a massless minimally coupled scalar field and a Yang-Mills field, coupled to each other only gravitationally.

The critical solution and the critical exponent γ for each system on its own are known. Both critical solutions are *discretely* self-similar (DSS), meaning they are periodic in the logarithm of spacetime scale with a period Δ, rather than continuously scale invariant. For both systems, the critical solution seen by fine tuning generic initial data has also been obtained by a DSS ansatz, and similarly the critical exponent has also been obtained from the linear perturbations of the resulting exactly DSS (critical) solution. The massless scalar field has $\Delta_{\rm scal} \simeq 3.44$ and $\gamma_{\rm scal} \simeq 0.37$ [1,18], while the Yang-Mills (YM) field has $\Delta_{\rm YM} \simeq 0.6$ and $\gamma_{\rm YM} \simeq 0.2$ [19,20].

Our system resembles the one recently considered by Kain [21], with the same YM field, but where the second matter field is a scalar field transforming as a triplet under the $SU(2)$ symmetry. The main difference is that those two matter fields are coupled directly already on flat spacetime, as well as (inevitably) gravitationally. As a consequence, while the triplet could consistently be switched off, the YM field cannot.[1] Kain finds approximately DSS critical solutions dominated by one or the other field but does not focus on the case in between where both fields are in some sense equally strong.

Another closely related system is the most general ansatz for the $SU(2)$ YM field compatible with spherical symmetry. This consists of a "sphaleronic" degree of freedom in addition to the "magnetic" one considered in Refs. [19,20] and in the present paper, and so again there are two wavelike matter fields. Critical collapse, including type II, in this system was investigated numerically by Maliborski and Rinne [22]. The full system has a global $U(1)$ symmetry, with a Mexican hat potential for the two fields. The magnetic field w and sphaleronic field ω can be reparametrized as $w + i\omega = Se^{i\phi}$. The purely magnetic dynamics are then recovered by setting ϕ to a constant. Our interpretation of the results in Sec. II. C of Ref. [22] is that type II critical collapse in the full system is dominated by the S critical solution (that is, the known critical solution for the purely magnetic system), with the dynamics of ϕ subdominant.[2]

II. COVARIANT FORM OF THE FIELD EQUATIONS

Our first matter field is the minimally coupled scalar field ψ, for which Choptuik [1] originally discovered critical phenomena. It obeys the four-dimensional wave equation

$$\Box_4\psi := \nabla_a\nabla^a\psi = 0. \tag{1}$$

This wave equation holds on arbitrary spacetimes, but here we always restrict to spherical symmetry. (We use latin letters for abstract indices and greek ones for coordinate-specific ones and gravitational units such that $c = G = 1$.)

Our second matter field is the purely magnetic hedgehog ansatz for an $SU(2)$ Yang-Mills field in spherical symmetry, which was famously considered for static solutions by Bartnik and Mckinnon [23] and later for critical collapse by Choptuik *et al.* [19]. This can be parametrized by a single spherically symmetric field W as

$$\begin{aligned} F = {} & dW \wedge (\tau_1 d\theta + \tau_2 \sin\theta d\varphi) \\ & - (1 - W^2)\tau_3 d\theta \wedge \sin\theta d\varphi, \end{aligned} \tag{2}$$

where τ_i are the Pauli matrices with $\mathrm{tr}\tau_i\tau_j = \delta_{ij}$ and (θ, φ) are the usual angles on the 2-spheres that are invariant under spherical symmetry. W then obeys an equation of motion that is the wave equation in the two-dimensional spacetime reduced by the spherical symmetry, with a potential term, namely

$$\Box_2 W := R^2\nabla_a(R^{-2}\nabla^a W) = -\frac{W(1 - W^2)}{R^2}. \tag{3}$$

Here, the scalar R is the area radius, so the area of the invariant 2-spheres is $4\pi R^2$. We stress that W and its equation of motion (3) are defined only in a spherically symmetric spacetime via the ansatz (2).

In a static spacetime, there are two stable ground state solutions $W = \pm 1$, while the third constant solution $W = 0$ is unstable. Any solution that is smooth at the origin must take the form $W = \pm 1 + O(R^2)$. We pick the ground state $W = 1$ and without loss of generality write

[1] We note, however, that a scaling analysis shows that in an asymptotically self-similar solution the direct coupling becomes negligible in the limit of arbitrarily small scales.

[2] We note also that a scaling analysis shows that the S and ϕ dynamics remain coupled in the limit of increasingly small scales along an approximately self-similar solution.

$$W = 1 + R^2\chi, \tag{4}$$

where now in any smooth solution χ is an even function of R and generically $\chi = O(1)$ at the origin, as is also the case for the scalar field ψ.

We write the spherically symmetric metric in relaxed notation as

$$g_{ab} = \mathrm{diag}(\perp g_{ab}, R^2\gamma_{ab}), \tag{5}$$

where γ_{ab} is the unit metric on the 2-sphere and $\perp$ denotes the projection orthogonal to the invariant 2-spheres. The Einstein equations are

$$G_{ab} = 8\pi(T^{(\psi)}_{ab} + T^{(W)}_{ab}), \tag{6}$$

where

$$T^{(\psi)}_{ab} = \tilde{T}^{(\psi)}_{ab} - \frac{1}{2} g_{ab}\tilde{T}^{(\psi)}, \tag{7}$$

$$\tilde{T}^{(\psi)}_{ab} = \nabla_a\psi\nabla_b\psi, \tag{8}$$

and

$$T^{(W)}_{ab} = \tilde{T}^{(W)}_{ab} - \frac{1}{4} g_{ab}\tilde{T}^{(W)}, \tag{9}$$

$$\begin{aligned}\tilde{T}^{(W)}_{ab} &= \mathrm{tr}F_{ab}F^{ab} \\ &= \mathrm{diag}(\perp\tilde{T}_{ab}, PR^2\gamma_{ab}),\end{aligned} \tag{10}$$

$$\perp\tilde{T}_{ab} = 2R^{-2}\nabla_a W\nabla_b W, \tag{11}$$

$$P = R^{-2}\nabla_a W\nabla^a W + R^{-4}(1 - W^2)^2. \tag{12}$$

The scalar P can be interpreted as the tangential pressure in spherical symmetry. $T^{(\psi)}_{ab}$ and $T^{(W)}_{ab}$ are conserved separately, and these conservation laws imply the equations of motion for ψ and W.

III. DOUBLE NULL COORDINATES

We shall use double-null coordinates, in terms of which the line element becomes

$$ds^2 = -2gR_{,v}dudv + R^2(d\theta^2 + \sin^2\theta d\varphi^2). \tag{13}$$

Here, g and R are functions of u and v only. This means that surfaces of constant u and v are both null and that the affinely parametrized null geodesics ruling the surfaces of constant u have tangent vector $\nabla^a u$. We fix the remaining gauge freedom $u \to \tilde{u}(u)$, $v \to \tilde{v}(v)$ by setting $R(0, v) = v/2$ and requiring that u is proper time at the regular center $R = 0$.

There are four algebraically independent components of the Einstein equations. From these, we select one which is an ordinary differential equation for g on the slices of constant u and another one which is a wave equation for R. The other two Einstein equations are then redundant (they are replaced by suitable boundary conditions at $R = 0$). We also have wave equations for ψ and χ.

The four field equations we use can be arranged in the following hierarchy:

$$\mathcal{D}(\ln g) = 4\pi R[\mathcal{D}\psi)^2 + 2(R\mathcal{D}\chi + 2\chi)^2], \tag{14}$$

$$\mathcal{D}(RR_{,u}) = -\frac{g}{2} + 2\pi g R^2\chi^2(2 + R^2\chi)^2, \tag{15}$$

$$\mathcal{D}(R\psi_{,u}) = -R_{,u}\mathcal{D}\psi, \tag{16}$$

$$\begin{aligned}\mathcal{D}(R^2\chi_{,u}) = &-2RR_{,u}\mathcal{D}\chi - 4\pi g R^2\chi^3(2 + R^2\chi)^2 \\ &- \frac{g}{2}R^2\chi^2(3 + R^2\chi).\end{aligned} \tag{17}$$

Here,

$$\mathcal{D}f := \frac{f_{,v}}{R_{,v}} \tag{18}$$

so that $\mathcal{D}$ is the derivative with respect to R along the null geodesics ruling the slices of constant u. Equations (14)–(17) can be solved for g, $R_{,u}$, $\psi_{,u}$, and $\chi_{,u}$ in the above order by the integration

$$\mathcal{I}f := \int f R_{,v} dv \tag{19}$$

along lines of constant (u, θ, φ), starting from the center. Because of factors of R, three of the startup conditions are selected by regularity at $R = 0$, and we fix the fourth condition by imposing the gauge choice $g = 1$ at $R = 0$. This selection and arrangement of equations resembles the form of the field equations for the spherical scalar field of [24–26] (but with $\mathcal{D}$ and $\partial/\partial u$ applied to ψ in the opposite order), and also the scheme of [27] for the vacuum Einstein equations on null cones with a regular vertex (but in terms of double null coordinates u and v, rather than Bondi coordinates u and R).

Using $dR = R_{,u}du + R_{,v}dv$, we can transform the metric (13) from the double-null coordinates (u, v) to the Bondi coordinates (u, R), obtaining

$$ds^2 = -2gdudR - Gdu^2 + R^2(d\theta^2 + \sin^2\theta d\varphi^2), \tag{20}$$

where

$$G := -2gR_{,u}. \tag{21}$$

At the center $R = 0$, we have $G = g^2$, and so, as already mentioned above, we impose $g = 1$ there in order to make u proper time along the worldline $R = 0$. The quantity $\sqrt{G}du$ is proper time along any curve of constant (R, θ, φ), and so $\sqrt{G}$ gives the redshift of photons traveling from the central $R = 0$ observer to other constant R and nonrotating observers, at constant retarded time u. We can also define the compactness $2M/R$, where M is the Hawking mass, as

$$\frac{2M}{R} \coloneqq 1 - \nabla_a R \nabla^a R = 1 + 2\frac{R_{,u}}{g}. \tag{22}$$

For the diagnosis of subcritical scaling, we define the stress-energy quantities

$$T_{(1)} \coloneqq \frac{2}{g}\psi_u \mathcal{D}\psi, \tag{23}$$

$$T_{(2)} \coloneqq \frac{2\sqrt{2}}{g}(R\chi_{,u} + 2R_{,u}\chi)(R\mathcal{D}\chi + 2\chi), \tag{24}$$

$$T_{(3)} \coloneqq \chi^2(2 + R^2\chi)^2. \tag{25}$$

These definitions are motivated by the identities $T^{a(\psi)}_{\ a} = T_{(1)}$ and $T^{(\psi)}_{ab}T^{ab(\psi)} = T^2_{(1)}$ for the scalar field and $T^{a(\chi)}_{\ a} = 0$ and $T^{(\chi)}_{ab}T^{ab(\chi)} = T^2_{(2)} + T^2_{(3)}$ for the YM field. (The square of the total stress energy is not a sum of squares).

IV. NUMERICAL METHOD

Our numerical implementation follows that of Ref. [26] (for similar, but not the same, field equations). We represent our fields on a grid at fixed values of v and numerically advance in the retarded time u.

At every time step, we make a least-squares fit $\psi \simeq \psi_0 + \psi_1 R + O(R^2)$ and $\chi \simeq \chi_0 + \chi_1 R + O(R^2)$ to the four innermost grid points where $R > 0$ (points where $R < 0$ are no longer evolved). We then substitute these expansions into the integral expressions for g, $R_{,u}$, $\psi_{,u}$, and $\chi_{,u}$, obtaining

$$g = 1 + 2\pi R^2(\psi_1^2 + 8\chi_0^2) + O(R^3), \tag{26}$$

$$R_{,u} = -\frac{1}{2} - \frac{\pi}{3}\psi_1^2 R^2 + O(R^3), \tag{27}$$

$$\psi_{,u} = \frac{1}{2}\psi_1 + O(R), \tag{28}$$

$$\chi_{,u} = \frac{1}{2}\chi_1 + O(R). \tag{29}$$

The truncations indicated denote generically nonvanishing terms that depend on the next-order expansion coefficients. This expansion is used for the first three grid points with $R > 0$ to start up the integration. For the remaining grid points, the integral $\mathcal{I}$ is discretized with respect to R by the trapezoid rule and $\mathcal{D}$ by symmetric finite differencing with respect to R between adjacent grid points, giving a scheme that is second-order accurate in v. (The grid values of v never appear explicitly; only those of R and the other fields do). R, χ, and ψ are evolved in u using the method of lines and specifically a second-order Runge-Kutta integrator, with the expansions and integrals reevaluated for each Runge-Kutta substep. After the completion of each full time step, we excise grid points with $R < 0$ and continue evolving only those with $R > 0$.[3]

The scheme as described so far is strictly causal, in the sense that information does not travel numerically outside the continuum light cones given by the lines of constant u and v. Considering u as the time coordinate, this means that information does not travel in the negative v direction. Therefore, no boundary condition is required either mathematically or numerically at the outer boundary $v = v_{\max}$.

Stability of a finite difference algorithm for a hyperbolic problem usually requires a limit on the ratio of the time step to the space step, commonly called the Courant factor. A necessary upper bound on the Courant factor is given by the requirement of causality; that is, all physical characteristics must lie inside the numerical domain of influence of the finite difference stencil. The upper bound on the Courant factor sufficient for numerical stability is typically lower than the necessary bound from causality by some factor of order unity. In double-null coordinates, by contrast, there is no upper bound on the Courant factor $\Delta u/\Delta v$ from causality, but of course some upper bound will still be required for numerical stability. A geometric condition involving only $\Delta u/\Delta v$ and the metric that can serve as an alternative to the causality condition is

$$|R_{,u}|\Delta u \le C R_{,v}\Delta v, \tag{30}$$

where C is a dimensionless factor of order unity (see also Ref. [25]). We implement this as

$$\Delta u = C \min_i \frac{2(R_i - R_{i-1})}{(R_{,u})_i + (R_{,u})_{i-1}}. \tag{31}$$

This is evaluated before each full time step. We find empirically that the method is stable for test fields on Minkowski spacetime for $C \le 2.8$ but unstable for $C \ge 3.0$, for 100, 200, 400, and 800 grid points, and so there seems to be a necessary and sufficient limit on C approximately independent of resolution, as was intended with the condition (30). As one would expect for violating a Courant condition, for C too large, the code blows up rapidly and at grid spatial frequency. Allowing for a large

[3]We do not change the spatial grid within each time step in order for the differentiability assumptions underlying the method of lines to hold.

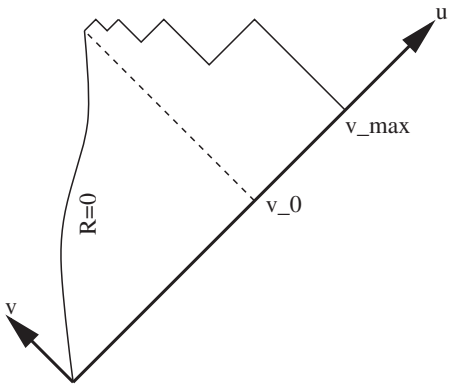

FIG. 1. Schematic plot of the numerical domain in the uv-plane, focusing on the regridding process. For simplicity, this domain has only three regriddings. The regular center $R = 0$ is not in general at $u = v$.

safety margin in strongly curved spacetimes, we have used $C = 0.1$ for all our nonlinear simulations. Note that only the matter wave equations are subject to a Courant condition at all, as the Einstein equations we solve are hypersurface equations solved by integration on time slices (more precisely, along outgoing null rays).

Although we use double-null coordinates, the fact that we have parametrized $g_{uv} = -gR_{,v}$ implies that our time evolution stops asymptotically as a marginally outer-trapped sphere is approached, indicated in our coordinates by $R_{,v} = 0$. We identify the formation of a black hole by the time step going below a predefined threshold, and we approximate the (Hawking) mass of the first outer-trapped sphere by $R/2$ at the grid point where $R_{,v}$ is minimal.

Following Garfinkle [26], we use a very simple form of mesh refinement adapted to the specific problem of critical collapse in spherical symmetry. We identify, by hand, the approximate value v_0 of v corresponding to the point of largest curvature, or the first outer-trapped sphere, in a suitable near-critical evolution within a given one-parameter family of initial data. Once half of the grid points with $v < v_0$ are excised because they have reached $R < 0$, we reuse the computer memory by fitting a new grid point in the middle between each existing grid point. We assign values of R, ψ, and χ to the new grid points by cubic Gauss interpolation, which for this simple arrangement gives (in terms of the new grid index)

$$f_i = \frac{9}{16}(f_{i+1} + f_{i-1}) - \frac{1}{16}(f_{i+3} + f_{i-3}). \tag{32}$$

In this regridding step, information can propagate to negative v by a distance of $(3/2)\Delta v_{\text{old}}$ (the width of the interpolation stencil). It would be possible to avoid this by setting field values at the new grid points by extrapolation from the left (smaller v), but we would expect this to be noisy, and so have not attempted it. We note that the regridding does not happen after a fixed number of time steps but at fixed moments of time independently of resolution and so should not be thought of as part of the underlying time evolution scheme. We also note that the numerical scheme remains exactly causal in the presence of regridding, in the sense that the new outer boundary point is obtained in the same way as the new interior points, and no outer boundary condition is required.

In contrast to Ref. [26], where v_0 and $v_{\max}$ are identical, we have $v_{\max} > v_0$, and we regrid by a factor of 2 also in $v_0 < v < v_{\max}$ after discarding the outer half of it. The resulting numerical domain is shown schematically in Fig. 1. Having the buffer outside of v_0 allows us to see what we would otherwise be missing by potentially making v_0 too small and seems to make the regridding more robust, at the cost of only an insignificant increase in computing time.

V. SIMILARITY SOLUTIONS

In any coordinates $x^\mu = (T, x, \theta, \varphi)$ adapted to spherical symmetry and to DSS, a spherically symmetric spacetime is DSS if and only if the metric takes the form

$$g_{\mu\nu} = e^{-2T}\tilde{g}_{\mu\nu}, \tag{33}$$

where $\tilde{g}_{\mu\nu}$ is periodic in T with some period Δ. In particular, the area radius R must take the form

$$R = e^{-T}\tilde{R}, \tag{34}$$

with $\tilde{R}$ again periodic.

A scalar-field ψ of which the stress-energy tensor is compatible with this metric must itself be periodic in T with the same period.

The equation of motion of χ (or W) is not compatible with exact DSS, but there are solutions which are asymptotically DSS on small scales as $T \to \infty$ and in which χ takes the form

$$\chi = e^{T}\tilde{\chi} \tag{35}$$

with $\tilde{\chi}$ asymptotically periodic as $T \to \infty$. In particular, the observed critical solution is of this form. In this limit, the two round brackets on the right-hand side of

$$-\frac{W(1-W^2)}{R^2} = \chi(1 + e^{-T}\tilde{R}^2\tilde{\chi})(2 + e^{-T}\tilde{R}^2\tilde{\chi}) \tag{36}$$

can be approximated by 1 and 2, respectively, as $T \to \infty$ in (34), turning (3) into

$$\Box_2(R^2\chi) = 2\chi. \tag{37}$$

(In flat spacetime in the usual coordinates, where $\Box_2 = -\partial_t^2 + \partial_r^2$, this equation is just $-\chi_{,tt} + \chi_{,rr} + 4r^{-1}\chi_{,r} = 0$, with the r^{-2} terms on both sides canceling.)

One could consistently truncate the equation of motion (3) for W to (37) and its conserved stress-energy tensor (9)–(12) by replacing (12) with

$$P = R^{-2}\nabla_a W \nabla^a W + 4\chi^2. \tag{38}$$

We do not do this here but rely on fine-tuning to make the solutions asymptotically DSS on small scales.

Based on our null coordinates, we define the specific DSS-adapted coordinates

$$x := \frac{R}{u_* - u}, \qquad T = -\ln(u_* - u), \tag{39}$$

for a constant $u_* > 0$ and $u < u_*$. (For $u > u_*$, both x and T are undefined.) From the form (20) of the metric, it is clear that the metric in coordinate (x, T) is of the form (33) and that the spacetime is discretely self-similar if and only if g and G are periodic in T. Hence, we will use (x, T) as auxiliary coordinates in the diagnosis of discrete self-similarity. In an (asymptotically) DSS solution, the metric quantity $2M/R$ is also periodic, and so are the matter fields ψ and $\tilde{\chi} = e^{-T}\chi$. We define the stress-energy scalars $\tilde{T}_{(i)} := e^{-2T}T_{(i)}$ which are periodic in DSS, except that the YM potential term $\tilde{T}_{(3)} = 4\tilde{\chi}^2(1 + O(e^{-T}))$ is only asymptotically periodic on small scales.

VI. NUMERICAL RESULTS

Following some rough initial experimentation, we have used the two-parameter family of initial data

$$\psi(0, v) = 0.075p(1 - q)e^{-\left(\frac{R-0.75}{0.25}\right)^2}, \tag{40}$$

$$\chi(0, v) = 0.25pqe^{-\left(\frac{R-0.3}{0.1}\right)^2}. \tag{41}$$

Recall also that we make the gauge choice $R(0, v) = v/2$. Here, $q = 0$ corresponds to pure scalar field data, and $q = 1$ corresponds to pure YM data. We have adjusted the other parameters so that for both $q = 0$ and $q = 1$ the critical value of p is $p_* \simeq 1$, and they have similar values of $v_0 \simeq 3.4$. We use $v_{\max} = 4$ (so that $0 \le R \le 2$ initially) and 401 grid points throughout.

We find that, for a given value of q, it is sufficient to carry out about 30 bisections without regridding in order to get a good enough estimate of v_0. We then fix v_0, (or rather, the corresponding grid point index i_0) and carry out 50 bisections from scratch with up to eight regriddings in each evolution. (The buffer $v_0 < v < v_{\max}$ allows us to do this without losing the accumulation point from the grid and without the need for the iterative refinement of v_0 described in Ref. [26]). This simple process gives us mass and curvature scaling down to the machine precision limit $|p - p_*| \simeq 10^{-15}$. It is remarkable that this takes only a few minutes of computation on a laptop, with negligible memory.

How many scale echoes we see in our most fine-tuned evolutions with $|p - p_*| \simeq 10^{-15}$ depends on both Δ and γ. For $q = 0$ (pure scalar), we expect to see DSS over a range $\Delta T \simeq 15 \cdot \ln 10 \cdot \gamma_{\text{scal}} \simeq 12.8$, corresponding to $\Delta T/\Delta_{\text{scal}} \simeq 3.5$ scale oscillations, and this is what we observe. Similarly, for $q = 1$ (pure YM), we get $\Delta T \simeq 15 \cdot \ln 10 \cdot \gamma_{\text{YM}} \simeq 6.9$, corresponding to $\Delta T/\Delta_{\text{YM}} \simeq 11.5$ scale oscillations.

We initially determine u_* as the approximate value of retarded time for black hole formation or largest curvature. We then plot $2M/R$, ψ, $\tilde{\chi}$, and the $\tilde{T}_{(i)}$ against the resulting x and T and further adjust u_* to make these as periodic in T as possible. (The $\tilde{T}_{(i)}$ are the most sensitive tool for this.) As a test of the correctness of our methods, we clearly see the expected number of oscillations at the correct periods and the expected scaling of the black hole mass and the curvature terms $T_{(i)}$ with the correct critical exponents, as well as the periodic "wiggle" in the curvature scaling laws that comes from DSS [18,28]. The scalar field ψ in the pure scalar field critical solution is shown in Fig. 2, and the compactness $2M/R$ of the corresponding spacetime in Fig. 3. The mass and curvature scaling laws in the pure scalar case are shown in Fig. 4. The rescaled YM field $\tilde{\chi}$ in the pure YM critical solution is shown in Fig. 5, and the compactness $2M/R$ of the corresponding spacetime in Fig. 6. The mass and curvature scaling laws in the pure YM case are shown in 7. (We plot $\ln M$ and $-1/2 \ln T_{(i)}$ against $\ln|p/p* - 1|$.)

We next add a YM test field to the scalar field critical solution and a scalar test field to the YM critical solution. (In practice, we evolve $q = \epsilon$ and $q = 1 - \epsilon$ with $\epsilon = 10^{-12}$. This still requires a small adjustment to p_* but makes no visible difference to the dominant field and metric, while the perturbation field obeys an essentially linear equation of motion.)

We can formally write the purely YM critical solution as $Z_{*\text{YM}}(x, T)$, which obeys

$$Z_{*\text{YM}}(x, T + \Delta_{\text{YM}}) = Z_{*\text{YM}}(x, T), \tag{42}$$

for the dependent variables $Z = (\tilde{\chi}, g, G, R)$. Separation of variables then allows us to consistently look for solutions of the scalar test field equation of the form

$$\psi(x, T) = e^{\lambda T}\psi_\lambda(x, T), \tag{43}$$

where $\psi_\lambda(x, T)$ is a complex mode function, with the same period Δ_{YM} in T as the background solution. The complex frequency λ arises from solving a boundary value problem, imposing periodicity of $\psi_\lambda(x, T)$ in T and regularity at the regular center and the past light cone of the singularity of the background spacetime. We expect a discrete set of complex conjugate pairs of such modes to exist. From a complex mode, a specific real solution is then obtained as

$$\psi(x, T) = \Re[e^{i\delta}e^{\lambda T}\psi_\lambda(x, T)], \tag{44}$$

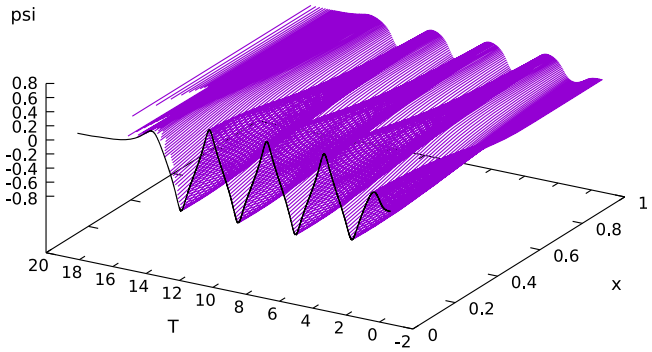

FIG. 2. The scalar field $\psi(x,T)$ for optimal fine-tuning with $q=0$ (only the scalar field is present). The regular center $x=0$ runs along the front edge of the graph, with the values of ψ there emphasized by a black line line.

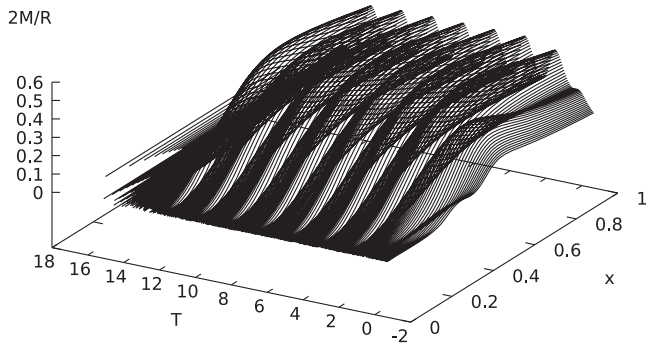

FIG. 3. The compactness $(2M/R)(x,T)$, defined in Eq. (22), for the same solution as in Fig. 2.

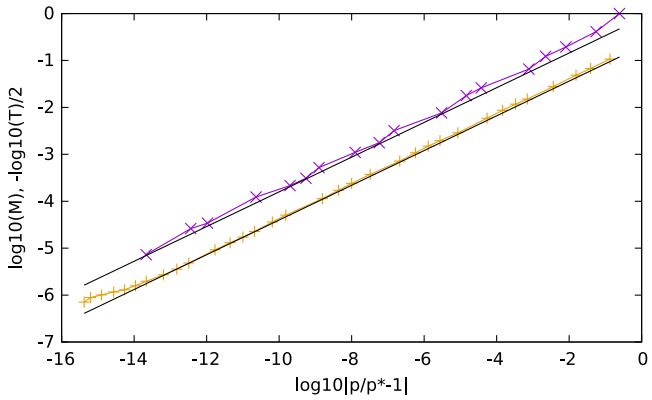

FIG. 4. Mass and curvature scaling laws for the pure scalar field. The upper curve (purple) represents $-(1/2)\log_{10}(\max T_{(1)})$, and the lower curve (orange) represents $\log_{10} M$, both against $\log_{10}|p/p_*-1|$. The straight gray lines corresponding to $\gamma=0.37$ are shown for comparison.

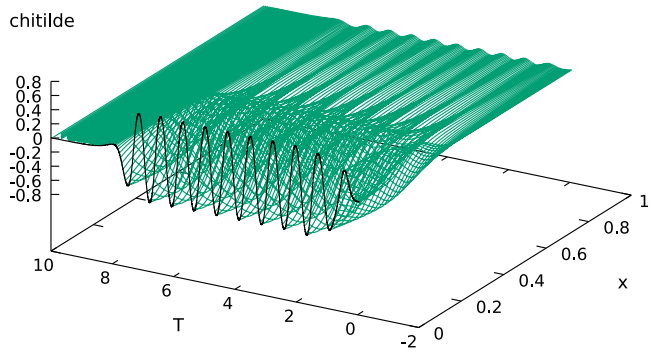

FIG. 5. The rescaled Yang-Mills function $\tilde{\chi}(x,T)$ [see Eqs. (4) and (35)] for optimal fine-tuning with $q=1$ (only the YM field is present). Note the range of T here $(-2<T<10)$ is not the same as in Fig. 2 $(-2<T<20)$. Again, the values of $\tilde{\chi}$ at the regular center $x=0$ are emphasized by a black line line.

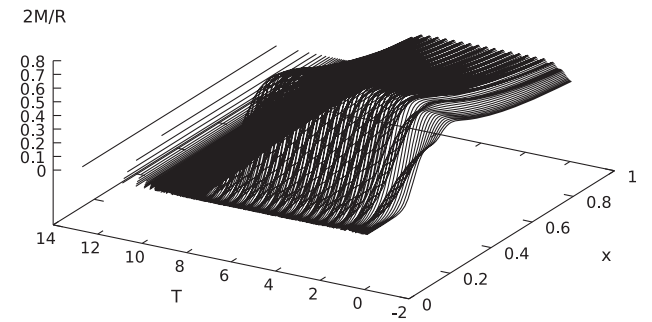

FIG. 6. The compactness $(2M/R)(x,T)$ for the same solution as in Fig. 5.

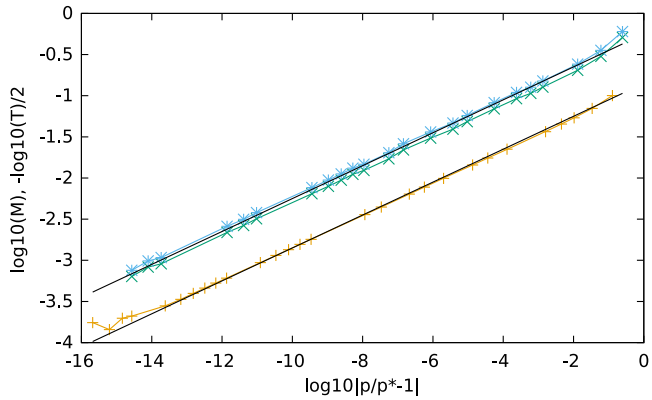

FIG. 7. Mass and curvature scaling laws for the pure YM field, as in Fig. 4 except that the two upper curves now show $T_{(2,3)}$ (green and blue). Gray lines $\gamma=0.20$ are shown for comparison.

for an arbitrary value of the phase δ. Similar expressions hold for a YM test field $\tilde{\chi}$ on the scalar field critical solution background with variables $Z=(\psi,g,G,R)$ and period Δ_{scal}.

A time evolution with generic initial data for the linear test field is dominated with increasing T by the mode or complex conjugate pair of modes with the largest real part of λ. Our numerical results are compatible with this theoretical result, with the dominant $\lambda=-0.40+3.7i$ for the YM field on the scalar field background and $\lambda=0.09+4.2i$ for the scalar field on the YM background.

To our surprise, the YM perturbation on the scalar field background decays, but the scalar field perturbation on the YM background grows exponentially in T.

Next, we explore the black hole threshold in our two-parameter set of initial data by fixing q and fine tuning p to its (q-dependent) critical value. For all values of q, we find a single critical solution that is "shared" by the two matter fields. There is complementary evidence for this from the scaling laws (varying p) on the one hand and from single "best" near-critical time evolutions (with a particular $|p/p_* - 1| \sim 10^{-15}$) on the other.

The evidence from varying p is that the black hole mass and the maximum values of the energy densities $T_{(i)}$ achieved in a given evolution show clear approximate power-law scaling with the same p_*. By "approximate" power-law scaling, we mean that the exponent γ for each fixed q depends weakly on $\ln|p_* - p|$. In a plot of $\ln M$ vs $\ln|p - p_*|$, this appears as an almost straight line. For $q = 0.9$, 0.92 and 0.93, we see a break in the slope, with the larger slope (larger γ) closer to the black hole threshold.

Figure 8 demonstrates this for $q = 0.92$, where the break is roughly in the middle of our fine-tuning range: at low fine-tuning (on the right), the YM field dominates the stress energy (recall we are plotting *minus* the log of $T_{(i)}$), and everything scales with $\gamma = 0.25$, while at high fine-tuning (on the left), the scalar field dominates, and everything scales with $\gamma = 0.33$. For $q = 0.9$, the critical exponent breaks from 0.25 to 0.37, and for $q = 0.93$, it breaks from 0.23 to 0.27. (These are all rough values fitted by eye, as illustrated in Fig. 8). By contrast, for $q = 0.95$, we see a constant critical exponent 0.22, with the YM field dominant throughout our fine-tuning range. Compare these values with 0.37 for the pure scalar field, $q = 0$, and 0.20 for the pure YM field, $q = 1$.

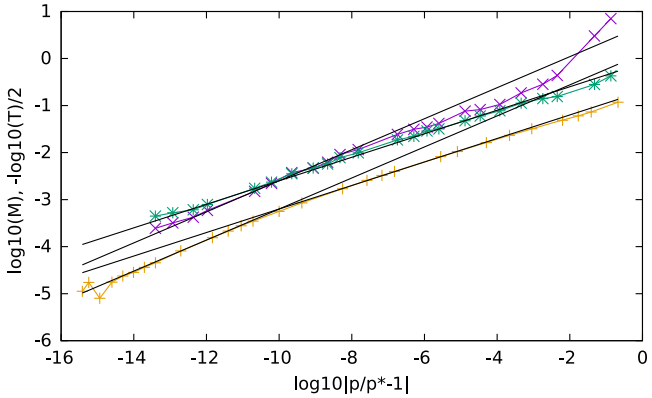

FIG. 8. Mass and curvature scaling laws for the mixed initial data with $q = 0.92$. As in Fig. 4 except that the two upper curves now show $T_{(1,2)}$ (purple and green). $T_{(3)}$ is not shown for clarity but is close to $T_{(2)}$, as it was in Fig. 7. There are now two pairs of straight gray lines for comparison, corresponding to $\gamma = 0.25$ and $\gamma = 0.33$. These illustrate a break in the scaling laws around $|p/p_* - 1| = 10^{-10}$.

The evidence from individual near-critical time evolutions is more complicated and is summarized in Figs. 9–11. The key observation is that we can always fit the coordinates x and T and the rescalings of χ to $\tilde{\chi}$ and the $T_{(i)}$ to $\tilde{T}_{(i)}$, with a single choice of the parameter u_* for all these variables and for both matter fields. The two matter fields share the same accumulation point of scale echoes, and their stress energies scale with the same factor $(u_* - u)^{-2}$.

However, all quantities that would be strictly periodic in one of the two single-field critical solutions are far from periodic in mixed-field near-critical evolutions. The spacetime observable $(2M/R)(x, T)$ switches over gradually with increasing T from the structure familiar from the pure YM solution (a maximum over x of around 0.7, with small-amplitude high-frequency modulation in T) to that of scalar field solution (a maximum over x of around 0.5, with large low-frequency modulation in T). This is illustrated for $q = 0.92$ in Fig. 9.

Moreover, ψ and its stress energy $\tilde{T}_{(1)}$ oscillate (in a quasiperiodic way) and grow in T, while $\tilde{\chi}$ and its stress energy $\tilde{T}_{(2,3)}$ oscillate and decay. Figure 10 illustrates this

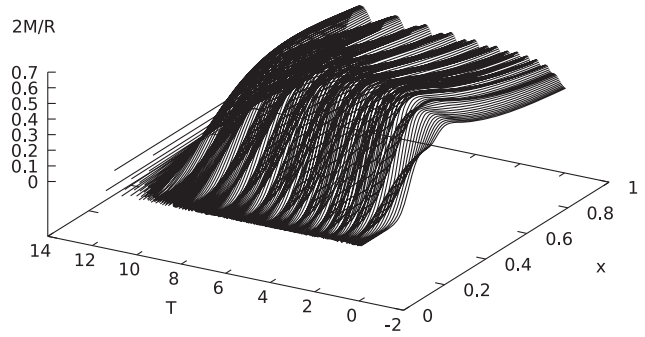

FIG. 9. The compactness $2M/R$ against x and T, in our best subcritical time evolution with $q = 0.92$.

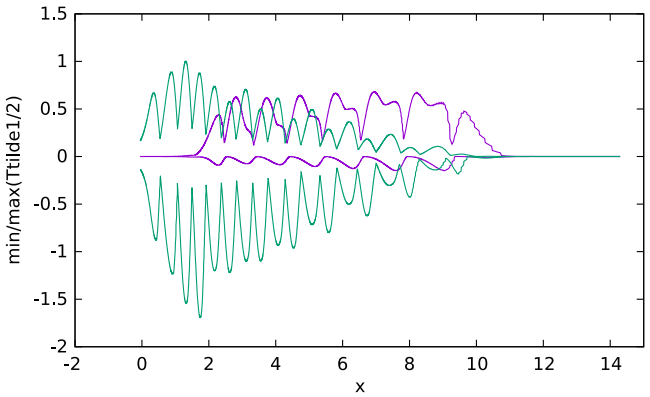

FIG. 10. $\min_x$ and $\max_x$ of $T_{(1)}$, (scalar field stress-energy, purple) and similarly for $T_{(2)}$ (YM kinetic stress-energy, green), against T, in our best subcritical time evolution with $q = 0.92$. We see that for small T this spacetime is dominated by the YM stress-energy, but that at large T it is dominated by the scalar field stress-energy.

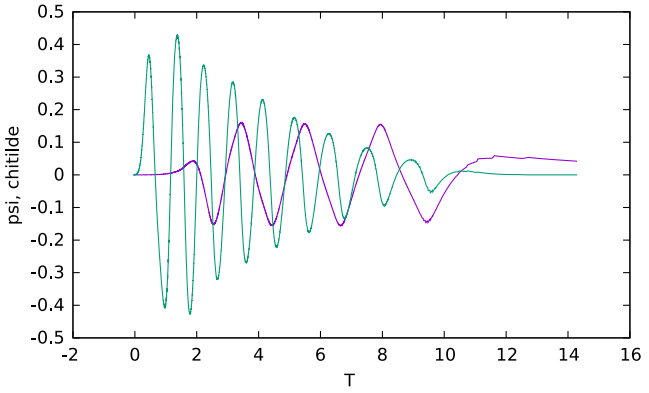

FIG. 11. ψ (scalar field, purple) and $\tilde{\chi}$ (rescaled YM field, green) at the origin, against T, in our most closely fine-tuned subcritical time evolution with $q = 0.92$. Consistently with Fig. 10, the YM field decays, and the scalar field takes over. Compare these curves with the periodic values at the origin $x = 0$ in the two single-field critical solutions, shown as the black lines in Figs. 2 and 5.

switchover from $\tilde{T}_{(2,3)}$ to $\tilde{T}_{(1)}$ during the evolution of near-subcritical initial data with $q = 0.92$. Figure 11 illustrates the fields ψ and $\tilde{\chi}$ generating these stress-energy sectors. These should be compared against Figs. 2 and 5.

For clarity, when we show both fields together, we do not plot against x and T, but only the maxima and minima of $\tilde{T}_{(1,2)}$ over x [in effect, a sideways view of the corresponding (x, T) plot], and the central values of ψ and $\tilde{\chi}$, all against T.

VII. CONCLUSIONS

The numerical limits of fine-tuning do not allow us to follow the putative critical solution for given q down to arbitrarily large T, but our observations are consistent with the assumption that in the limit of perfect fine-tuning our time evolutions for all $0 < q < 1$ are heading toward a critical solution that ends in a curvature singularity as $T \to \infty$, with the scalar field increasingly dominant as T increases.

Moreover, we conjecture that there is a family of fully nonlinear solutions that start from the pure YM critical solution at $T \to -\infty$ and end at the pure scalar field critical solution at $T \to \infty$, which show the scaling of the metric and matter fields with respect to an accumulation point u_* typical of similarity solutions but where the spacetime is scale periodic with a definite period (DSS) only in the limits $T \to \pm\infty$. (This period is Δ_{YM} as $T \to -\infty$ and the YM field dominates, and Δ_{scal} as $T \to \infty$ and the scalar field dominates.)[4] In between, they are at best quasiperiodic, in the sense that we expect a Fourier transform in T to show broad frequency peaks around multiples of both $2\pi/\Delta_{\mathrm{scal}}$ and $2\pi/\Delta_{\mathrm{YM}}$. We propose the term quasiperiodically self-similar (QSS) for such solutions. (In our numerical experiments, we have not obtained this solution for a large enough range of T to usefully take such a Fourier transform. Rather, we appeal to Fig. 9 to illustrate what we mean by QSS, in contrast to Figs. 3 and 6, which show approximately DSS spacetimes.)

We can be more specific about the size of this family of solutions if we assume that at the YM starting point, where the scalar field is a test field, this test field can be approximated by the most rapidly growing (largest $\Re\lambda > 0$) mode of the form (43). There is then only a one-parameter family of such QSS solutions, parametrized by the constant phase δ in (44). Modulo this assumption, we conjecture that the critical solutions we find at different q by fine-tuning p are sections of this one-parameter family of QSS solutions, for starting values of T and values of δ that depend on q. (The range of T seen depends on the degree of fine-tuning we can achieve).

Our main evidence for this conjecture consists of the following observations: (1) at small q the YM field dominates down to the best fine-tuning we can manage (but the subdominant scalar field grows exponentially); (2) at large q the scalar field dominates from the beginning of the DSS phase (and the YM field continues to decay exponentially); (3) in an intermediate range of $0.90 \lesssim q \lesssim 0.93$ the scalar field takes over within the observed range of T; and (4) for smaller q it does so at larger T.

This model can be summarized in the schematic phase space picture of Fig. 12. Here, any point in the phase space is an initial dataset, up to an overall length scale, parametrized in our case as $(\psi(x), \tilde{\chi}(x))$, and a time evolution curve corresponds to a spacetime, in our case in null slicing, again up to an overall scale, with the time T of the dynamical system determining the missing scale as e^{-T}. In this picture, a DSS solution should be a closed curve, but for simplicity, we represent it as a fixed point. Similarly, we represent the conjectured one-parameter family of QSS solutions (parametrized by the phase δ) as a single curve.

Within the combined Einstein-YM-scalar system in spherical symmetry, the pure YM critical solution then has two unstable modes, and the pure scalar field has only one. However, the phase space picture illustrates that the QSS solution linking the two has itself only one unstable mode, which points out of the black hole threshold toward either collapse or dispersion. Hence, we conjecture that it acts as the critical solution for the combined Einstein-YM-scalar system, except in the limit where the scalar field is absent.

Before doing this numerical work, we had expected that both the scalar field and YM critical solution would be stable against perturbation by the other field. One would

[4]An exactly DSS solution for the YM field exists only in the limit $T \to \infty$ where $\tilde{\chi}$ varies over spacetime scales much smaller than the length scale set by the dimensionful YM self-coupling constant. Hence, if we talk about the YM critical solution as $T \to -\infty$ (large scales), we really mean the critical solution for the simplified matter model (37), (38) in which the YM field self-coupling is ignored.

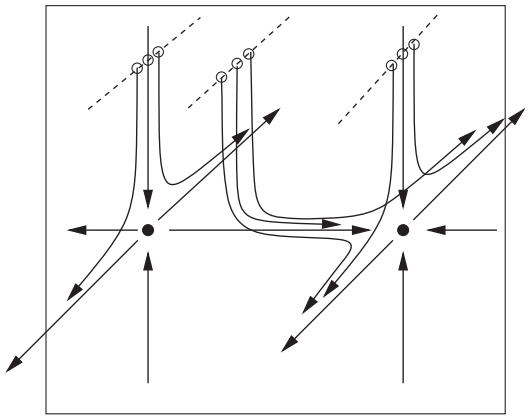

FIG. 12. Schematic conjectured phase space picture, with the infinite-dimensional phase space represented in three dimensions. The framed plane represents the black hole threshold (in reality a hypersurface). All arrow lines represent trajectories (spacetimes). The filled dots represent fixed points (DSS spacetimes): the YM critical solution, with two unstable modes, on the left, and the scalar critical solution, with one unstable mode, on the right. An infinite number of phase space dimensions of the black hole threshold are suppressed, and with them an infinite number of stable modes of each fixed point within the black hole threshold are suppressed. The horizontal straight arrow line linking the two represents the QSS solution conjectured in the Conclusions. The three dashed lines represent three families of initial data with $q = 0$ (left), $q = 1$ (right), and an intermediate value of q (middle). Hollow dots represent initial data with $p < p_*$, $p = p_*$ and $p > p_*$ for each family.

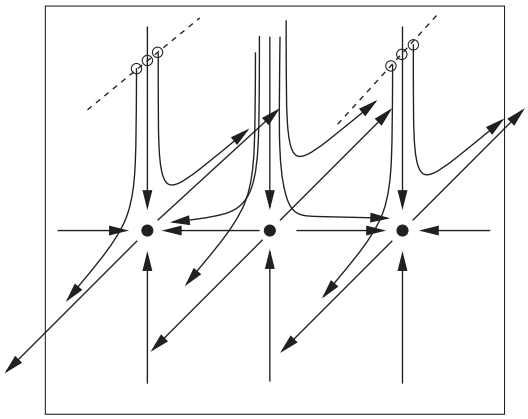

FIG. 13. An alternative hypothetical phase space picture. Here, the middle fixed point has two unstable modes, while the left and right ones have one each. This picture is definitely *not* realized for the spherical Einstein-YM-scalar system investigated in this paper but might be realized for another system with two competing massless fields.

then have expected there to be a third, two-mode unstable DSS solution in which both matter fields were present and which could be found by fine-tuning two parameters to some (p_*, q_*) with $0 < q_* < 1$.[5] The corresponding (hypothetical) more conservative phase space picture is shown in Fig. 13.

The unexpected results from our toy model highlight the question of which, if any, of those two qualitative phase space pictures is realized for a matter field such as electromagnetism, scalar, YM, or a perfect fluid, coupled to the Einstein equations in axisymmetry.

The only evidence that we have so far is that the spherically symmetric critical solutions for the perfect fluid[6] [30] and the scalar field [31] are linearly stable to all gravitational wave perturbations.[7] Unfortunately, we do not yet have good enough numerical simulations of axisymmetric vacuum gravitational collapse in order to investigate any axisymmetric Einstein-matter system in the opposite regime where the gravitational wave content dominates the matter stress energy, but we hope that our toy model and phase space pictures may be helpful in the interpretation of future results for such systems.

ACKNOWLEDGMENTS

This research was supported through the program Research in Pairs by the Mathematisches Forschungsinstitut Oberwolfach in 2019. It is a pleasure to thank the institute and its staff for hospitality during our stay. This work was also supported in parts by NSF Grant No. PHYS-1707526 to Bowdoin College, as well as through sabbatical support from the Simons Foundation (Grant No. 561147 to T. W. B.). D. H. is supported by the FCT (Portugal) IF Programs No. IF/00577/2015 and No. PD/BD/135511/2018. The authors would also like to acknowledge networking support by the COST Action GWverse Grant No. CA16104.

[5]Dynamically, such a solution $(\psi, \tilde{\chi}, g, G, R) = Z_{*,\mathrm{mixed}}(x, T)$ might have been of the two-oscillator form found in the context of boson stars in Ref. [29], meaning that its Fourier transform in T would show *sharp* peaks at multiples of two incommensurate scale frequencies.

[6]Assuming a linear equation of state $P = k\rho$, for the parameter range $0 < k \lesssim 0.49$.

[7]In fact, they are stable against all nonspherical perturbations, except for one unstable $\ell = 1$ perturbation associated with fluid rotation in the perfect fluid with $0 < k < 1/9$.

[1] M. W. Choptuik, Phys. Rev. Lett. **70**, 9 (1993).
[2] C. R. Evans and J. S. Coleman, Phys. Rev. Lett. **72**, 1782 (1994).
[3] C. Gundlach and J. M. Martín-García, Living Rev. Relativity **10**, 5 (2007).
[4] T. W. Baumgarte and C. Gundlach, Phys. Rev. Lett. **116**, 221103 (2016); Phys. Rev. D **94**, 084012 (2016); **97**, 064006 (2018).
[5] T. W. Baumgarte and P. J Montero, Phys. Rev. D **92**, 124065 (2015); J. Celestino and T. W. Baumgarte, Phys. Rev. D **98**, 024053 (2018).
[6] M. W. Choptuik, E. W. Hirschmann, S. L. Liebling, and F. Pretorius, Phys. Rev. D **68**, 044007 (2003).
[7] T. W. Baumgarte, Phys. Rev. D **98**, 084012 (2018).
[8] J. Healy and P. Laguna, Gen. Relativ. Gravit. **46**, 1722 (2014).
[9] N. Deppe, L. E. Kidder, M. A. Scheel, and S. A. Teukolsky, Phys. Rev. D **99**, 024018 (2019).
[10] K. Clough and E. A. Lim, arXiv:1602.02568.
[11] A. M. Abrahams and C. R. Evans, Phys. Rev. Lett. **70**, 2980 (1993); Phys. Rev. D **49**, 3998 (1994).
[12] D. Hilditch, A. Weyhausen, and B. Brügmann, Phys. Rev. D **96**, 104051 (2017).
[13] M. Alcubierre, G. Allen, B. Brügmann, E. Seidel, and W.-M. Suen, Phys. Rev. D **62**, 124011 (2000).
[14] D. Garfinkle and G. C. Duncan, Phys. Rev. D **63**, 044011 (2001).
[15] O. Rinne, Ph. D. thesis, University of Cambridge, 2005, arXiv:gr-qc/0601064.
[16] E. Sorkin, Classical Quantum Gravity **28**, 025011 (2011).
[17] D. Hilditch, T. W. Baumgarte, A. Weyhausen, T. Dietrich, B. Brügmann, P. J. Montero, and E. Müller, Phys. Rev. D **88**, 103009 (2013).
[18] C. Gundlach, Phys. Rev. D **55**, 695 (1997).
[19] M. W. Choptuik, T.Chmaj, and P. Bizón, Phys. Rev. Lett. **77**, 424 (1996).
[20] C. Gundlach, Phys. Rev. D **55**, 6002 (1997).
[21] B. Kain, Phys. Rev. D **99**, 104017 (2019).
[22] M. Maliborski and O. Rinne, Phys. Rev. D **97**, 044053 (2018).
[23] R. Bartnik and J. Mckinnon, Phys. Rev. Lett. **61**, 141 (1988).
[24] D. S. Goldwirth and T. Piran, Phys. Rev. D **36**, 3575 (1987).
[25] C. Gundlach, R. Price, and J. Pullin, Phys. Rev. D **49**, 890 (1994).
[26] D. Garfinkle, Phys. Rev. D **51**, 5558 (1995).
[27] R. Gómez, P. Papadopoulos, and J. Winicour, J. Math. Phys. (N.Y.) **35**, 4184 (1994).
[28] S. Hod and T. Piran, Phys. Rev. D **55**, R440 (1997).
[29] M. W. Choptuik, R. Masachs, and B. Way, Phys. Rev. Lett. **123**, 131101 (2019).
[30] C. Gundlach, Phys. Rev. D **65**, 084021 (2002).
[31] J. M. Martín-García and C. Gundlach, Phys. Rev. D **59**, 064031 (1999).